(12) INTERNATIONAL APPLICATION PUBLISHED UNDER THE PATENT COOPERATION TREATY (PCT)

(19) World Intellectual Property Organization
International Bureau

(43) International Publication Date
02 November 2023 (02.11.2023)

WIPO | PCT

(10) International Publication Number
WO 2023/210026 A1

(51) International Patent Classification:
G01N 27/30 (2006.01) *G01N 27/416* (2006.01)

(21) International Application Number:
PCT/JP2022/020301

(22) International Filing Date:
26 April 2022 (26.04.2022)

(25) Filing Language: English

(26) Publication Language: English

(71) Applicants: **THE UNIVERSITY OF TOKYO** [JP/JP]; 3-1, Hongo 7-chome, Bunkyo-ku, Tokyo 1138654 (JP). **CENTRE NATIONAL DE LA RECHERCHE SCIENTIFIQUE** [FR/FR]; 3, rue Michel Ange, 75016 Paris (FR).

(72) Inventors: **KIM, Soo Hyeon**; c/o The University of Tokyo, 3-1, Hongo 7-chome, Bunkyo-ku, Tokyo 1138654 (JP). **LI, Shuo**; c/o The University of Tokyo, 3-1, Hongo 7-chome, Bunkyo-ku, Tokyo 1138654 (JP). **FUJII, Teruo**; c/o The University of Tokyo, 3-1, Hongo 7-chome, Bunkyo-ku, Tokyo 1138654 (JP). **CLEMENT, Nicolas**; c/o CENTRE NATIONAL DE LA RECHERCHE SCIENTIFIQUE, 3, rue Michel Ange, 75016 Paris (FR).

(74) Agent: **TAZAKI, Akira** et al.; 1-9-2, Marunouchi, Chiyoda-ku, Tokyo 1006620 (JP).

(81) Designated States *(unless otherwise indicated, for every kind of national protection available)*: AE, AG, AL, AM, AO, AT, AU, AZ, BA, BB, BG, BH, BN, BR, BW, BY, BZ, CA, CH, CL, CN, CO, CR, CU, CZ, DE, DJ, DK, DM, DO, DZ, EC, EE, EG, ES, FI, GB, GD, GE, GH, GM, GT, HN, HR, HU, ID, IL, IN, IR, IS, IT, JM, JO, JP, KE, KG, KH, KN, KP, KR, KW, KZ, LA, LC, LK, LR, LS, LU, LY, MA, MD, ME, MG, MK, MN, MW, MX, MY, MZ, NA, NG, NI, NO, NZ, OM, PA, PE, PG, PH, PL, PT, QA, RO, RS, RU, RW, SA, SC, SD, SE, SG, SK, SL, ST, SV, SY, TH, TJ, TM, TN, TR, TT, TZ, UA, UG, US, UZ, VC, VN, WS, ZA, ZM, ZW.

(84) Designated States *(unless otherwise indicated, for every kind of regional protection available)*: ARIPO (BW, GH, GM, KE, LR, LS, MW, MZ, NA, RW, SC, SD, SL, ST, SZ, TZ, UG, ZM, ZW), Eurasian (AM, AZ, BY, KG, KZ, RU, TJ, TM), European (AL, AT, BE, BG, CH, CY, CZ, DE, DK, EE, ES, FI, FR, GB, GR, HR, HU, IE, IS, IT, LT, LU, LV, MC, MK, MT, NL, NO, PL, PT, RO, RS, SE, SI, SK, SM, TR), OAPI (BF, BJ, CF, CG, CI, CM, GA, GN, GQ, GW, KM, ML, MR, NE, SN, TD, TG).

Published:
— *with international search report (Art. 21(3))*

(54) Title: SENSOR

[Figure 1a]

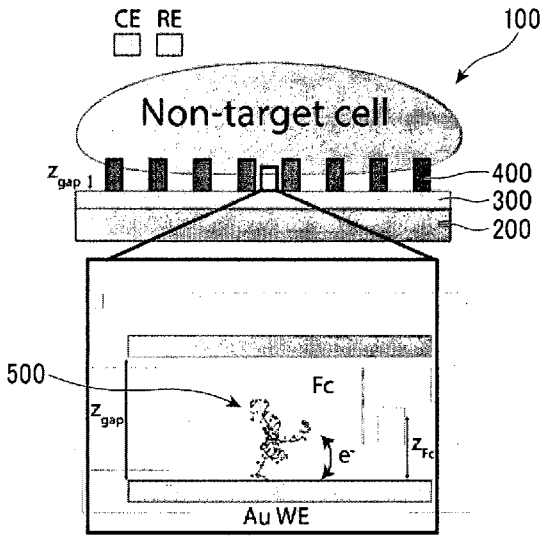

(57) Abstract: A sensor comprising: a substrate; an electrode being formed on at least a surface of the substrate; a pillar being formed on a surface of the electrode; and a sensing element formed on the surface of the electrode, and comprising an aptamer, wherein a length of the aptamer is shorter than a height of the pillar in direction perpendicular to the surface of the electrode.

WO 2023/210026 A1

[DESCRIPTION]

[Title of the Invention]

SENSOR

[Technical Field]

[0001]

The present invention relates to sensor.

[Background Art]

[0002]

Cancer is still one of the main pathologies with high probability of negative prognostic (death) in humans. In the search for a personalized, high-precision medicine, in recent years much effort has been directed toward realizing cancer detection transducers and lab-on-a-chip devices aiming at implementing new strategies for cancer early detection and treatment, for instance by targeting rare circulating tumor cells (CTCs).

[0003]

These sensors are typically based on physical-chemical effects such as fluorescence, chemiluminescence, magnetic beads, calorimetry profiling or electrochemistry. Generally speaking, electrochemical sensors provide attractive means for easy operation, high sensitivity, and portability. Additionally, they can benefit from ultimate scaling, either using redox-cycling or high-frequency signal amplification effects, as illustrated by the successful launch of ECsens startup for detecting individual biomarker particles specifically.

[Citation List]

[Patent Literature]

[0004]

[PTLt 1] Japanese Patent No. 6485855

[Summary of Invention]

[Technical Problem]

[0005]

However, despite these progresses, the transfer of bioelectrochemical sensors from proteins or small biomarker particles to cells is not a straightforward path. For

example, the abundant literature on e-DNA sensors, based on the grafting of redox-labelled aptamers and used for protein detection, contrasts with the lack of studies at the cell level with these redox-labelled sensors.

[0006]

Therefore, the present invention has been made in view of the above problems, and an object of the present invention is to provide a redox-labelled sensor being able to improve signal to noise ratio.

[Solution to Problem]

[0007]

The present invention has been made based on the above findings, and the gist is as follows.

[0008]

[1] A sensor comprising:

a substrate;

an electrode formed on at least a surface of the substrate;

a pillar formed on a surface of the electrode; and

an aptamer formed on the surface of the electrode,

wherein a length of the aptamer in hairpin configuration is shorter than a height of the pillar in direction perpendicular to the surface of the electrode.

[2] The sensor according to [1],

wherein a height of the pillar is 5 nm to 40 nm, and a length of the aptamer is 10 nm to 30 nm.

[3] The sensor according to [1] or [2],

wherein the pillar comprises a surface being parallel to the surface of the electrode and being placed apart from the surface of the electrode.

[4] The sensor according to [1] to [3],

wherein the pillar is made of a dielectric material.

[5] The sensor according to [1] to [4],

wherein the electrode is one or more selected from the group consisting of a metal, a semiconductor, and a carbon material.

[6] The sensor according to [1] to [5],

wherein the aptamer is selected from the group consisting of a nucleic acid aptamer, a peptide aptamer, a protein aptamer, and a peptide nucleic acid.

[7] The sensor according to [1] or [6], further comprising:

a redox label being attached to the aptamer.

[8] The sensor according to [7],

wherein the redox label is ferrocene.

[9] The sensor according to [5],

wherein the electrode is Au.

[10] The sensor according to [4],

wherein the pillar is hydrogen-silsesquixane nanopillar.

[11] The sensor according to anyone of [1] to [10], further comprising:

a circuit for processing electron signal generated by the sensing element.

[Advantageous Effects of Invention]

[0009]

As described above, according to the present invention it is possible to provide a redox-labelled sensor being able to improve signal to noise ratio.

[Brief Description of Drawings]

[0010]

[Fig. 1(a)] FIG. 1(a) is schematic representation of the sensor composed of nanopillars suspending non-target cells according to embodiment of the present invention.

[Fig. 1(b)] FIG. 1(b) is schematic representation of the sensor composed of nanopillars suspending target cells according to embodiment of the present invention.

[Fig. 1(c)] FIG. 1(c) is Atomic Force Microscope (AFM) image and cross section of the HSQ nanopillars according to Example of the present invention.

[Fig. 1(d)] FIG. 1(d) is schematic representation of the Cyclic Voltammetry (CV/CVs) the embodiment of the present invention.

[Fig. 2(a)] FIG. 2(a) is graph showing results of CVs of a sensor measured until 14 days according to Example of the present invention.

[Fig. 2(b)] FIG. 2(b) is graph showing results of CVs of 10 different sensor with same fabrication condition according to Example of the present invention.

[Fig. 3(a)] FIG. 3(a) is graph showing AFM cross section and CV according to Example of the present invention.

[Fig. 3(b)] FIG. 3(b) is graph showing AFM cross section and CV according to Example of the present invention.

[Fig. 4] FIG. 4 is figure showing schematic representation of the sensor and CVs according to Example of the present invention.

[Fig. 5(a)] FIG. 5(a) is graph showing CV according to Example of the present invention.

[Fig. 5(b)] FIG. 5(b) is graph showing CV peaks (I_{peak}) plotted as a function of cells concentration according to Example of the present invention.

[Fig. 6(a)] FIG. 6(a) is graph showing hydrogen bonds energy estimated from MD simulation of tethered SYL3C aptamers without confinement, and under 5nm confinement according to Example of the present invention.

[Fig. 6(b)] FIG. 6(b) is graph showing I_{peak} plotted as a function of temperature for unconfined SYL3C, confined SYL3C with Ramos cells, and confined SYL3C with Capan-2 cells.

[Fig. 7] FIG. 7 is graph showing results of stability test for CVs of the sensor with only Aptamer modified with Ferrocene (Apt-Fc) molecules obtained in 1.5 h according to Example of the present invention.

[Fig. 8] FIG. 8 is fluorescent image to show the capan-2 cells clusters on the surface of our sensor after incubation according to Example of the present invention.

[Fig. 9(a)] FIG. 9(a) is graph showing CVs of Apt-Fc under confinement with Ramos cells according to Example of the present invention.

[Fig. 9(b)] FIG. 9(b) is graph showing CVs of Apt-Fc unconfined according to Example of the present invention.

[Fig. 9(c)] FIG. 9(c) is graph showing CVs of Apt-Fc under confinement with Capan-2 cells according to Example of the present invention.

[Fig. 10] FIG. 10 is images showing the cell concentration and cell size.

[Description of Embodiments]

[0011]

Hereinafter, an embodiment of the present invention will be described in detail with reference to the attached drawings. In addition, in this specification and the drawings, like constituent elements having substantially the same function and configuration are denoted by like reference numerals, and redundant description will be omitted.

[0012]

Throughout the specification and claims, the following terms take the meanings explicitly associated herein, unless the context clearly dictates otherwise. The terms "coupled" and "connected", which are utilized herein, are defined as follows. The term "connected" is used to describe a direct connection between two circuit elements, for example, by way of a metal line formed in accordance with normal integrated circuit fabrication techniques. In contrast, the term "coupled" is used to describe either a direct connection or an indirect connection between two circuit elements. For example, two coupled elements may be directly coupled by way of a metal line, or indirectly connected by way of an intervening circuit element (e.g., a capacitor, resistor, or by way of the source/drain terminals of a transistor). The term "circuit" means either a single component or a multiplicity of components, either active or passive, that are coupled together to provide a desired function. The term "signal" means at least one current, voltage, or data signal. Should the invention involve a stacked chip arrangement, the front sides of two chips may be directly connected since the electrical interconnects on each chip will most commonly be formed on the front sides of each chip, or the front side of one chip may be directly

connected to the backside of the second, which may employ through chip interconnects. Although circuit elements may be fabricated on the back side, when reference is made to certain circuit elements residing within or formed in a substrate, this is generally accepted to mean the circuits reside on the front side of the substrate.

[0013]

<<Sensor>>

First, a sensor 100 according to an embodiment of the present invention will be described in detail. The sensor 100 includes: a substrate 200; an electrode 300 being formed on at least a surface of the substrate 200; a pillar 400 being formed on a surface of the electrode 300; and a sensing element 500 formed on the surface of the electrode, and including an aptamer 510, wherein a length of the aptamer 510 is shorter than a height of the pillar 400 in direction perpendicular to the surface of the electrode 300.

[0014]

<Substrate>

FIG. 1(a) is schematic representation of the sensor composed of nanopillars suspending non-target cell according to embodiment of the present invention. As shown in FIG. 1(a), the sensor 100 includes the substrate 200. The substrate 100 at least has one surface (A). The substrate 100 may be plate shape or sheet shape. A material of the substrate 100 may be at least one or more selected from the group consisting of a dielectric material, a semiconductor material, and conductor material. In the FIG. 1(a), the substrate 100 is semiconductor material. When the substrate 100 is semiconductor material, circuits can be from on the surface (A) of the substrate 100 and buried in the substrate 100. Thereby, the sensor 100 can be more compact. The substrate 100 may be flexible substrate 100.

[0015]

<Electrode>

As shown in FIG. 1(a), the sensor 100 includes the electrode 300. The electrode 300 is formed on the surface (A) of the substrate 200. The electrode 300 has one surface (A) that is different from a surface being in touch with the surface (B) of the substrate 200. The electrode 300 may be plate shape or sheet shape.

The electrode 300 is one or more selected from the group consisting of a metal, a semiconductor, and a carbon material. In FIG. 1(a), the electrode 300 is Au.

[0016]

<Pillar>

As shown in FIG. 1(a), the sensor 100 includes the pillar 400. The pillar 400 is formed on the surface (B) of the electrode 300. The pillar 400 is for supporting a cell. Thereby, the pillar 400 ensures that the cell is too close with the sensing element 500. Thus, noise by cells gravity or cells stickiness can be further decreased. Therefore, signal to noise ratio can be further improved. The pillar 400 may include a surface being parallel to the surface of the electrode and being placed apart from the surface of the electrode 300.

[0017]

There can be two or more of pillars 400 formed on the surface (B) of the electrode 300. Therefore, the pillar 400 can support a cell more certainly. A pillar array may be form on the surface (B) of the electrode 300. The pillar array may be a regular array. A height of the pillar may be 5 nm to 40 nm. Thereby, noise by cells gravity or cells stickiness can be further decreased. The diameter between the pillars may be 200 nm or more. Thereby, penetration of pillars in the cell membrane can be avoided.

[0018]

The pillar may be made of a dielectric material. In FIG. 1(a), the pillar 400 is hydrogen-silsesquioxane (HSQ) nanopillars.

[0019]

<Sensing element>

As shown in FIG. 1(a), the sensor 100 includes the sensing element 500. The sensing element 500 may include the aptamer 510, and a redox label 520. The sensing element 500 is formed on the surface (B) of the electrode 300. That is, the sensing element 500 is formed on the same surface of the electrode 300 as the pillar 400.

[0020]

(Aptamer)

The length of the aptamer 510 is shorter than the height of the pillar in direction perpendicular to the surface of the electrode. The aptamer 510 is oligonucleotide or peptide molecules that bind to a specific target molecule. The aptamer 510 can be one or more selected from the group consisting of a nucleic acid aptamer, a peptide aptamer, a protein aptamer, and a peptide nucleic acid. The nucleic acid aptamer can be a DNA aptamer or RNA aptamer. In FIG. 1(a), the aptamer 510 is DNA aptamer. The length of the aptamer 510 may be 10 nm to 30 nm.

[0021]

(Redox label)

The redox label 520 may be attached to the aptamer 510. A type of the redox label 520 is not limited. In FIG. 1(a), the redox label 520 is ferrocene.

[0022]

According to the sensor 100 of the present embodiment, as the pillar 400 ensures that the cell is too close with the sensing element 500, noise by cells gravity or cells stickiness can be further decreased. Therefore, signal to noise ratio can be further improved.

[Example]

[0023]

Hereinafter, an Example of the present invention will be described in detail with reference to the attached drawings.

[0024]

(Aptamer electrochemical cytosensor with nanosupported cells)

FIG. 1(a) is schematic representation of the sensor composed of nanopillars suspending non-target cells according to embodiment of the present invention. It is composed of: 1) a gold working electrode; 2) an active monolayer, composed of tethered Ferrocene (Fc)-labelled DNA aptamers (the experimentally identified SYL3C) deposited on a gold surface, for the recognition of the Epithelial Cell Adhesion Molecule (EpCAM), also including oligoethylene-glycol molecules (OEG) to avoid non-specific adsorption; and 3) a regular array of hydrogen-silsesquioxane (HSQ) nanopillars. The regular array of hydrogen-silsesquioxane (HSQ) nanopillars

is fabricated by high-speed electron-beam (e-beam) lithography, used to improve the signal to noise ratio of e-DNA cytosensors.

[0025]

The HSQ solution is cross-linked to form a SiOx network structure after the exposure, which provides a chemically stable, flat, and biocompatible pattern. The diameter of 200 nm for the pillars has been chosen to avoid penetration of pillars in the cell membrane. Pillars pitch and height depend on cell deformation between pillars, and the length of the DNA aptamers dispersed on the surface between the pillars. The 500 nm pitch was chosen on the basis of a theoretical cell adhesion/deformation phase diagram as well as high yield fabrication process, as small pillar height requires a dense configuration. The atomic force microscope (AFM) image shown in FIG. 1(c) presents the optimized nanopillars configuration with 200 nm diameter, 20 nm height and 500 nm pitch aiming to keep cells at a distance z_{gap} of few nanometers above the surface, small enough to enable interaction of SYL3C aptamers with EpCAMs (FIG.1(b)).

[0026]

FIGs. 1(a), and 1(b) depict how the aptamer Brownian motion affects the charge transfer between Fc and the electrode. Typical Cyclic Voltammetry (CV) curves are shown in FIG. 1(d). As a first order approximation, one can say that when aptamers interact with the EpCAM, the Brownian motion is partially stopped, and the Fc molecule cannot transfer charges near the surface (FIG.1(b)). Out-of-equilibrium voltammograms can be observed when the CV sweep rate is faster than electron transfer or diffusion rate (relative to the motion through z_{gap}). Given the simple nature of the structure under study, molecular dynamics simulations can be used to support the analysis of experimental results, as will be discussed later. FIGs.1(a), and 1(b) illustrate the full atomistic molecular dynamics representation of SYL3C aptamers, as well as the EpCAM interacting with SYL3C.

[0027]

First, we show the good stability and controllability of the studied electrochemical aptasensor. up to 14 days and with 10 aptasensors (FIGs. 2(a) and 2(b)). The optimum configuration has been obtained when mixing thiolated Fc-

aptamers with thiolated OEG (OEG-SH), following an approach similar to the one introduced by Herne et al. but with OEG-SH instead of mercapto-hexanol. Such a mixed monolayer approach aims to get an as complete as possible surface coverage combining DNA with small molecules to avoid any DNA desorption. Monolayers composed of only DNA led to poor stability performances in CV (FIG. 7).

[0028]

The last tunable parameter is the pillars height that can be controlled precisely with HSQ. We used lymphoma cell line (Ramos), that do not express EpCAM, as a reference for supported cells without specific molecular recognition. FIGs.3(a), 3(b) and 4(a) show CVs obtained for 7.1, 17.6 and 20 nm pillars height, respectively, while FIG.4(b) shows CVs without any pillars, both in the absence and presence of Ramos cells. While the CV peak (I_{peak}) is unaffected by the presence of Ramos cells for 20 nm thick pillars, I_{peak} is decreased with smaller pillar heights, suggesting that cells are "pushing" on the aptamer layer. We stress that only few nanometers change in pillars height have a strong effect on CVs. We attribute I_{peak} decrease with pillar's height to the fact that cells act as a dielectric layer. The redox oxidation potential cannot be reached due to the tiny/high impedance channel between Fc molecules and CE/RE, an effect related to the "current blocking" exploited in some label-free electrochemical biosensors. Such an effect disappears with 20 nm pillar height.

[0029]

To confirm the specific molecular recognition of EpCAM with SYL3C using our 20 nm thick nanopillar electrochemical sensor, we used pancreatic cancer cells (Capan-2), which have a high level of EpCAM expression. We see, as expected, that I_{peak} is strongly decreased when inserting Capan-2 cells, unlike for Ramos cells (FIGs.4a,c). A similar I_{peak} decrease is observed for non-supported cells, but the results are more difficult to be quantified in this case as non-target cells also contribute to decreasing I_{peak}, leading to a decrease in signal to noise ratio (FIG.4(b),(d)). This nano-supported cells electrochemical device shows an excellent linear sensor response to Capan-2 cells spreading over 2 orders of magnitude (FIG. (5)). It is observed that CV peaks decreased with increasing Capan-2 concentrations within the range from 5×10^3 cells/mL to 1×10^6 cells/mL (number of cells range from 25 to 5000 incubated

with the device). By fitting the extracted oxidized peak current in -FIG.4(c) with $I = 7.567 - 0.995 \times \log C$ (cells/mL), $R^2 = 0.964$, the lower limit of detection (LOD) of the proposed method in the microfluidic was calculated to be 13 cells. We believe that the LOD is presently limited by the formation of cell clusters (FIG.5 (b), inset, and FIG. 8), which is likely related to the logarithmic dependence of I_{peak} with C in FIG.5 following the Brunauer, Emmett and Teller (BET) adsorption model.

[0030]

(Aptamer Brownian motion: nanoconfinement effect)

The possibility to suppress cells gravity effect offers additional opportunities. For example, the simplicity of the molecular assembly and nanopillars configuration enables a direct link between experimental electrochemical results and molecular dynamics computer simulations, even in complex environment containing living cells. As a result of the computer simulations, it is found that lateral nanoconfinement can be a precious degree of freedom to tune the hairpin melting temperature. FIG.6a shows the hydrogen bond energy histogram for tethered SYL3C at different temperatures in the absence/presence of a 5 nm confinement. This energy is related to the number of base pairs formed by the single-strand DNA, and therefore to the various hairpin configurations. The unconfined tethered SYL3C shows three main peaks at 20 °C, whereas only low energy peaks are observed above 40 °C, as expected from the 3 and 1-2 hairpins SYL3C configurations (FIG.6a).

[0031]

In contrast, the hydrogen bond energy distribution for tethered SYL3C under confinement shows only low energy peaks configuration, suggesting for a lower melting temperature due to the confinement effect. Experimental measurements on tethered SYL3C aptamer with temperatures varying between 25 and 70 °C show indeed a clear difference between confined aptamers (Ramos cells act as a top of the confined channel without specific interaction) and free aptamers (FIG.6b). I_{peak} for tethered SYL3C under confinement does not vary much with temperature (CVs are shown in FIGs.9(a), (b), (c)), as expected from the weak temperature dependent aptamer configuration (FIG.6a). In that case, I_{peak} remains at its maximum value because all Fc, associated with aptamer Brownian motion in confined space, have a

chance to exchange electrons to the bottom electrode. In other words, I_{peak} is only related to the number of aptamers on the surface. In contrast, I_{peak} decreases with temperature for unconfined SYL3C that can be associated with a decreased probability of electron transfer to the bottom electrode (the unconfined single-hairpin configuration extends Fc-surface distance).

[0032]

Finally, I_{peak} decreases substantially with the temperature in the presence of Capan-2 cells. This is related to the mechanism illustrated in FIG.1b with blocked electron transfer due to specific molecular recognition with aptamer folded DNA, Fc remaining close to the cell interface during recognition and cannot reach the bottom electrode. Therefore, I_{peak} decrease can be related statistically to the percentage of aptamers interacting with the cell, a process that is thermally activated. Discussion on "cell gravity" signal to noise and temperature effects the present device with suspended cells improves signal to noise ratio as it suppresses the parasitic signal arising from non-target cells (FIGs. 4a,b), clearly pointing out what we can call a "cell gravity" issue. Interestingly, previously reported electrochemical cytosensors (beyond e-DNA sensors) were typically based on a more complex architecture involving several self-assembly steps and nanoparticles.

[0033]

One can argue that these nanoparticles, once on the surface, are playing a role analogue to the HSQ nanopillars introduced here. The nanopillar approach has the merit to simplify the assembly process, to control perfectly z_{gap}, and to be compatible with an aggressive downscaling/integration with many nanoelectrodes. It is also compatible with other nanoelectrochemical sensing approach including the one introduced by ECsens, so far based on biological systems smaller than 2 microns. Future versions of the device will be developed in multiple electrode configurations, thus enabling statistical analysis at the single-cell level, exploiting our single-cell trapping lab-on-chip. The gravity issue being solved, the actual limit of detection is the nonfaradic capacitance arising from the sensing nanolayer, that is proportional to the active area. As 13 cells correspond to about 1/1000 of the active area in the present experiment, the use of sensing area matching exactly to a single-cell with microwells

should enable to get high signal to noise ratio at the single-cell level. The absolute I_{peak} value is expected to be in the tens of pA for a single cell, which could be measured with commercial equipment. Interestingly, the recent breakthrough in electrochemistry instrumentation allowing CVs at the aA level would be directly beneficial to the present sensing approach, allowing sub-cellular (and potentially single-molecule) studies with nanoelectrodes in the 10 nm-range.

[0034]

A second advantage is related to the temperature dependence associated with the confinement effect. These devices aim to be implemented at the single-cell level, providing statistical distributions related to target and non-target cells populations. As a result, the relevant signal is ΔI_{peak} = I_{peak} (target cell) - I_{peak} (non-target) cell. According to FIG.6b, the difference in signal ΔI_{peak} is increasing significantly with temperature as I_{peak} related to non-target cells doesn't depend on temperature (as opposed to unconfined aptamers).

[0035]

Finally, confinement-induced hairpin melting temperature reduction is clearly observed in molecular dynamics simulations for SYL3C and is consistent with experimental data. This effect has some similarities with the recent report of duplex weakening when placed in a nanocage. The exact underlying mechanism remains to be unveiled in future studies. Hairpin weakening under nanoconfinement is very attractive for SYL3C aptamer, and probably many other aptamers, because the optimum aptamer folded configuration for specific molecular recognition is typically obtained at 37 °C with the SELEX method. Therefore, from a sensor perspective, it is better to operate near room temperature without the need for placing the sensor in an incubation chamber at 37 °C.

[0036]

FIG.6b illustrates this with a clear change in ΔI_{peak} observed at 30 °C, with cells simply inserted in a microfluidic channel without any prior incubation. In conclusion, we report a novel nano-electrochemical biosensor that uses nanopillar arrays to efficiently suppress the issue of cell gravity effect. The stability and efficiency of this device is illustrated for the detection of EpCAM expressed in

pancreatic cancer cells. Selectivity and sensitivity are illustrated over 3 orders of magnitude. The next device generation will be focusing on single-cell and potentially sub-cellular or single-molecule measurements, thereby offering unprecedented statistical analysis for the detection of rare cells such as CTCs. Molecular dynamics and experimental data presented here suggest that confinement significantly improves signal to noise ratio and affects aptamers melting temperature. Such an effect is a precious degree of freedom to optimize molecular interactions at near room temperature.

[0037]

(Methods and materials)

Preparation of self-assembled DNA/OEG mixed monolayers:

The Silicon wafer deposited with 20 nm gold/2 nm Ti (Au/Ti/Si) was cleaned in Acetone with sonication for 5 min, followed by rinsing with Isopropyl alcohol, deionized water and drying with nitrogen gas. Then, the cleaned chip was immersed in the freshly prepared solution of 1 mM OEG-SH in pure ethanol (containing an ethylene glycol repeat unit $HS(CH_2)_3(OCH_2CH_2)_6OCH_2COOH$, purchased from Prochimia) for 1 h and cleaned with ethanol, then immersed in 1 μM ssDNA-Fc solution, i.e., thiolated SYL3C aptamer dissolved in 0.5 M potassium phosphate solution (pH 8) for 2 h to obtain the mixed self-assembled monolayer surface. The aptamer sequence was as follows: ferrocene-5′-CAC TAC AGA GGT TGC GTC TGT CCC ACG TTG TCA TGG GGG GTT GGC CTG-$(CH_2)_3$-3′-SH (purchased from Biomers). The density of the probes was estimated to be about 2×10^{13} aptamers/cm^2 from the CV curves after background subtraction. The OEG or PEG backfilling approach is known to drastically reduce biofouling and thus nonspecific protein adsorption. The sample was cleaned with a solution of 0.05% Tween 20 for 10 s before use.

[0038]

Fabrication of Hydrogen silsesquioxane (HSQ) Nanopillars:

Hydrogen silsesquioxane (HSQ, Dow Corning XR-1541) negative electron beam (e-beam) resist is used to fabricate the nanopillars by using e-beam lithography; in this work the Advantest F7000s-VD02 e-beam machine is used. The HSQ resist

in a carrier solvent of MIBK was spin-coated on the Au/Ti/Si subtracted with acceleration 5000 rpm for 60 s and then baking at 150 °C for 2 min. The cured sample was then loaded in the e-beam machine and was exposed with a dose of 500 $\mu C/cm^2$ by using the on the fly (OTF) mode. The exposed sample was finally immersed in the alkali developer NMD-3 (TMAH 2.38%) for 5 min and then cured at 150 °C for 5 min to obtain the desired nanopillar array. The design of HSQ nanopillars dimension is followed the theory in ref.

[0039]

Cell Culture:

Both Capan-2 (Human Pancreas Adenocarcinoma cell line) and Ramos cells (Burkitt lymphoma cell line) were purchased from the cell library. Capan-2 and Ramos cells were cultured in RPMI 1640 medium supplemented with 10% fetal bovine serum (FBS) and 100 mg/mL penicillin-streptomycin) in a 5% CO_2 atmosphere at 37 °C. The cells were collected and separated from the medium by centrifugation at 1000 rpm, 4 °C for 5 min, and then were resuspended in a sterile PBS solution (pH 7.1), to obtain a homogeneous cell suspension. The cell suspension was prepared just before incubating with device. The cell number and cell size (Figure 10) were determined using a Petroff-Hausser Vcell counting chamber.

[0040]

Detection of cells:

There are two approaches applied for the detection of cells. One is that the cell suspension with fixed concentration was loaded in the device and then incubated in a 5% CO_2 atmosphere at 37 °C for 30 mins, experimental results are shown in the FIGs. 2-5. Another approach is that the cell suspension was loaded in the device without any further incubation. The experimental results are shown in the FIG. 9. For checking the cells with florescence microscopy, the cells were dyed with Calcein-AM.

[0041]

Electrochemical measurements:

The Metrohm Autolab and Princeton Applied Research Versastat 4 equipment were used for the electrochemical measurements. Commercial teflon cell with a bath

(FIGs.4b,4d,7) or with a microfluidic channel (FIGs.2,3,4a,4c,5a,9) from ALS company were used to set the sample and connected the output of the equipment to do the measurements. Cyclic voltammetry (CV) was selected for demonstrating the formation of the sensing probes and cells detection. A potential range of -0.1 V to -0.65 V vs Ag/AgCl, scan rate was varied from 0.5 to 5 V/s. For the density of the molecules on the electrode surface, the values were calculated by subtracting the blank values obtained from the capacitance.

[0042]

Calculation of the LOD:

The LOD of biosensor is determined by using the calibration curve of the device as shown in FIG.5b. Based on the ref. LOD is calculated using the equation $LOD = f^{-1}(y_{blank} - 3\sigma)$ by considering three times the standard deviation σ of the blank measurement, where f^{1} is the fitting function $I = 7.567 - 0.995 \times logC$ (cells/mL) obtained from the calibration curve, σ is equal to 0.15 from the experiments.

[0043]

Molecular dynamics simulations (MD):

Coarse grained MD oxDNA simulations were performed using the sequence dependent version of the model presented by B.E.K. Snoden et al. using SYL3C sequence. A Langevin thermostat was considered as well as electrostatic forces at each base corresponding to 0.1 M ionic strength (that of PBS). Tethered DNA is achieved with a punctual attractive harmonic potential on the first base, while a repulsion plane is considered to mimic the WE surface as well as the confinement induced by the cell. Simulations were performed for a duration of 10 μs with 909 fs steps. The orientational dependence of the interactions between the nucleotides captures the planarity of bases, of importance for formation of helical duplexes. The coaxial stacking term captures stacking interactions between bases that are not immediate neighbors along the backbone of a strand. Hydrogen-bonding interactions are possible only between complementary, Crick-Watson (A-T and C-G) base pairs, with the additional condition of approximate antialignment of the phosphodiester linkage, which leads to the formation of double helical structures. Bases and backbones also have excluded volume interactions, as well as backbones interactions.

[0044]

It should be noted that the embodiments of the present technology are not limited to the abovementioned embodiments, and various modifications can be made without departing from the gist of the present technology.

[0045]

Reference throughout this specification to "one embodiment," "an embodiment," "one example," or "an example" means that a particular feature, structure, or characteristic described in connection with the embodiment or example is included in at least one embodiment or example of the present invention. Thus, the appearances of the phrases such as "in one embodiment" or "in one example" in various places throughout this specification are not necessarily all referring to the same embodiment or example. Furthermore, the particular features, structures, or characteristics may be combined in any suitable manner in one or more embodiments or examples. Directional terminology such as "top", "down", "above", "below" are used with reference to the orientation of the figure(s) being described.

[0046]

Also, the terms "have," "include," "contain," and similar terms are defined to mean "comprising" unless specifically stated otherwise. Particular features, structures or characteristics may be included in an integrated circuit, an electronic circuit, a combinational logic circuit, or other suitable components that provide the described functionality. In addition, it is appreciated that the figures provided herewith are for explanation purposes to persons ordinarily skilled in the art and that the drawings are not necessarily drawn to scale.

[Industrial Applicability]

[0047]

According to the present invention, it is possible to provide a sensor being able to improve signal to noise ratio.

[Reference Signs List]

[0048]

sensor 100

substrate 200

electrode 300

pillar 400

sensing element 500

aptamer 510

[CLAIMS]

[Claim 1]

A sensor comprising:

a substrate;

an electrode being formed on at least a surface of the substrate;

a pillar being formed on a surface of the electrode; and

a sensing element formed on the surface of the electrode, and comprising an aptamer,

wherein a length of the aptamer is shorter than a height of the pillar in direction perpendicular to the surface of the electrode.

[Claim 2]

The sensor according to Claim 1,

wherein a height of the pillar is 5 nm to 40 nm, and a length of the aptamer is 10 nm to 30 nm.

[Claim 3]

The sensor according to Claim 1 or 2,

wherein the pillar comprises a surface being parallel to the surface of the electrode and being placed apart from the surface of the electrode.

[Claim 4]

The sensor according to anyone of Claims 1 to 3,

wherein the pillar is made of a dielectric material.

[Claim 5]

The sensor according to anyone of Claims 1 to 4,

wherein the electrode is one or more selected from the group consisting of a metal, a semiconductor, and a carbon material.

[Claim 6]

The sensor according to anyone of Claims 1 to 5,

wherein the aptamer is one or more selected from the group consisting of a nucleic acid aptamer, a peptide aptamer, a protein aptamer, and a peptide nucleic acid.

[Claim 7]

The sensor according to anyone of Claims 1 or 6,

wherein the sensing element further comprises a redox label being attached to the aptamer.

[Claim 8]

The sensor according to Claim 7,

wherein the redox label is ferrocene.

[Claim 9]

The sensor according to Claim 5,

wherein the electrode is Au.

[Claim 10]

The sensor according to Claim 4,

wherein the pillar is hydrogen-silsesquixane nanopillar.

[Claim 11]

The sensor according to anyone of Claims 1 to 10, further comprising:

a circuit for processing electron signal generated by the sensing element.

[Figure 1a]

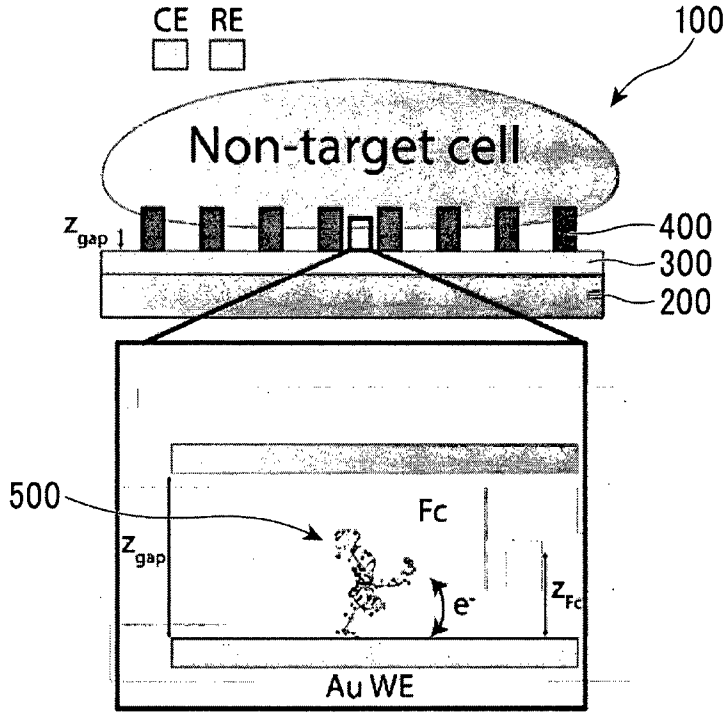
CE
RE
100
Non-target cell
$Z_{gap\ 1}$
400
300
200
500
Fc
Z_{gap}
e^-
Z_{Fc}
Au WE

[Figure 1b]

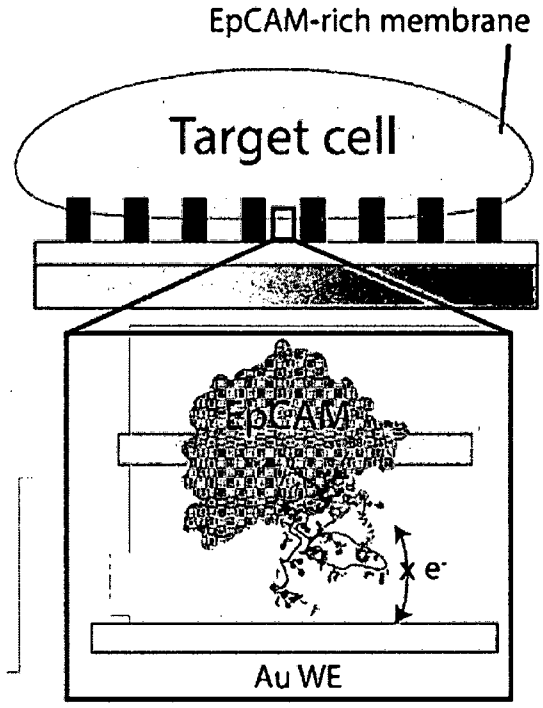

[Figure 1c]

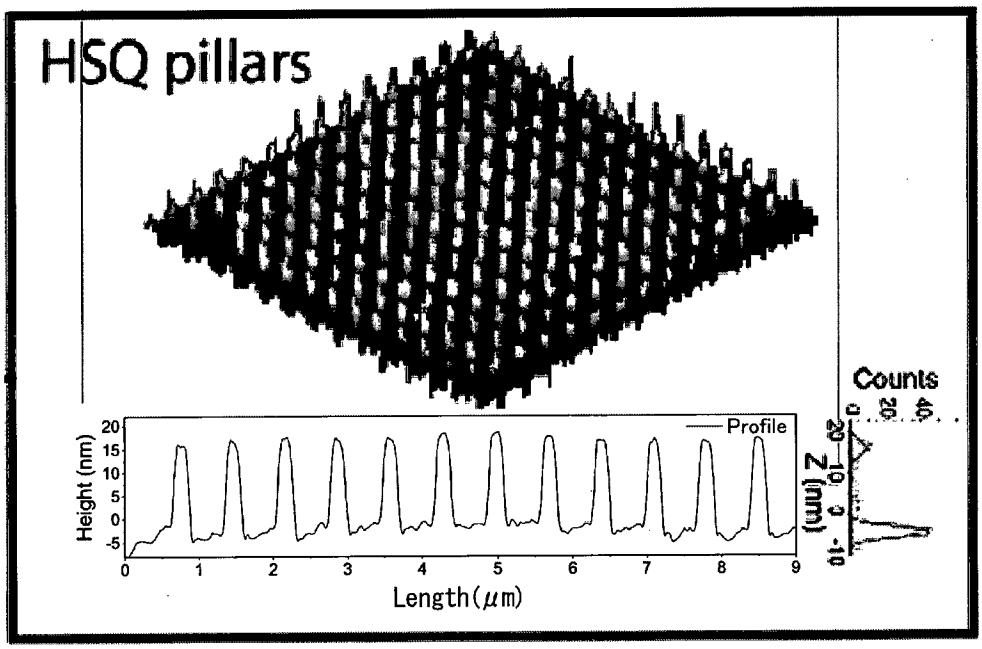
HSQ pillars
Profile
Height (nm)
20
15
10
5
0
-5
0
1
2
3
4
5
6
7
8
9
Length(μm)
Counts
Z (nm)

[Figure 1d]

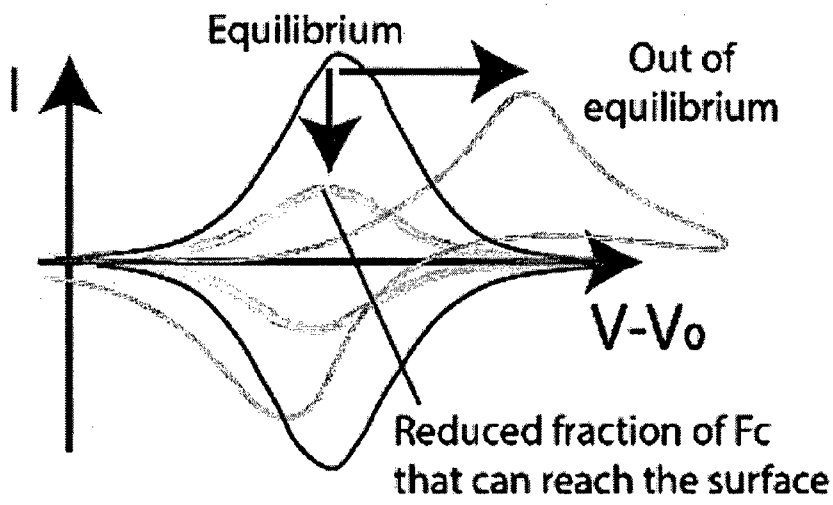
Equilibrium
Out of equilibrium
I
V-Vo
Reduced fraction of Fc that can reach the surface

[Figure 2a]

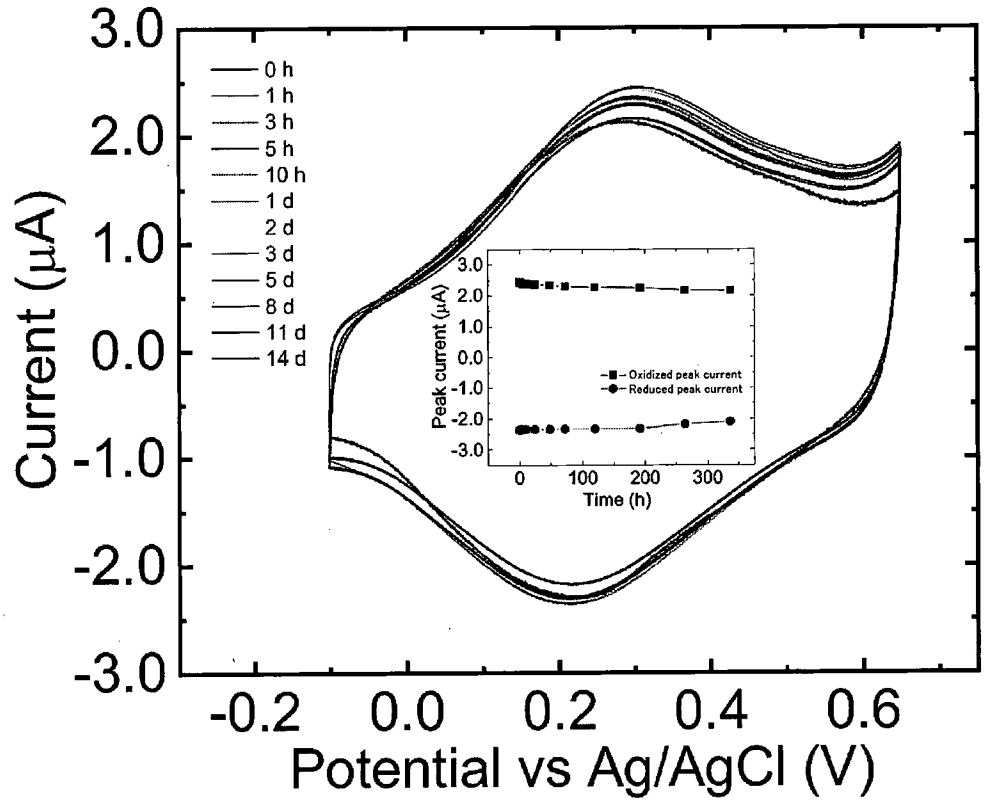
Current (μA)
Potential vs Ag/AgCl (V)
0 h
1 h
3 h
5 h
10 h
1 d
2 d
3 d
5 d
8 d
11 d
14 d
Peak current (μA)
Time (h)
Oxidized peak current
Reduced peak current

[Figure 2b]

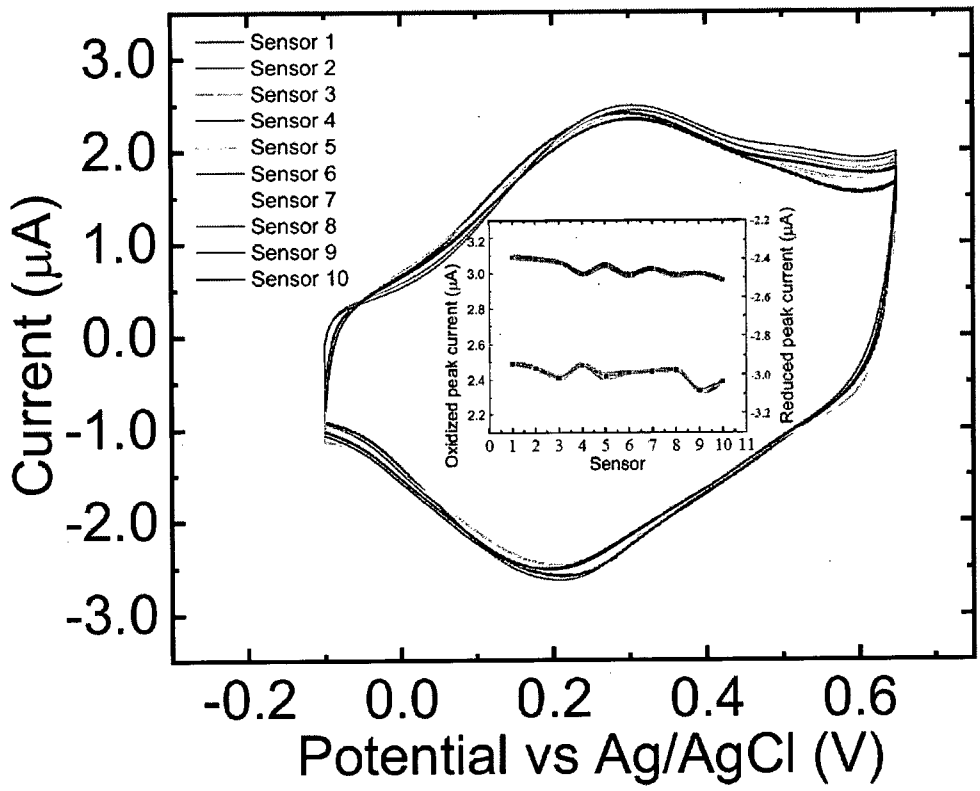
Sensor 1
Sensor 2
Sensor 3
Sensor 4
Sensor 5
Sensor 6
Sensor 7
Sensor 8
Sensor 9
Sensor 10
Current (μA)
3.0
2.0
1.0
0.0
-1.0
-2.0
-3.0
-0.2
0.0
0.2
0.4
0.6
Potential vs Ag/AgCl (V)
Oxidized peak current (μA)
Reduced peak current (μA)
Sensor
0 1 2 3 4 5 6 7 8 9 10 11

[Figure 3a]

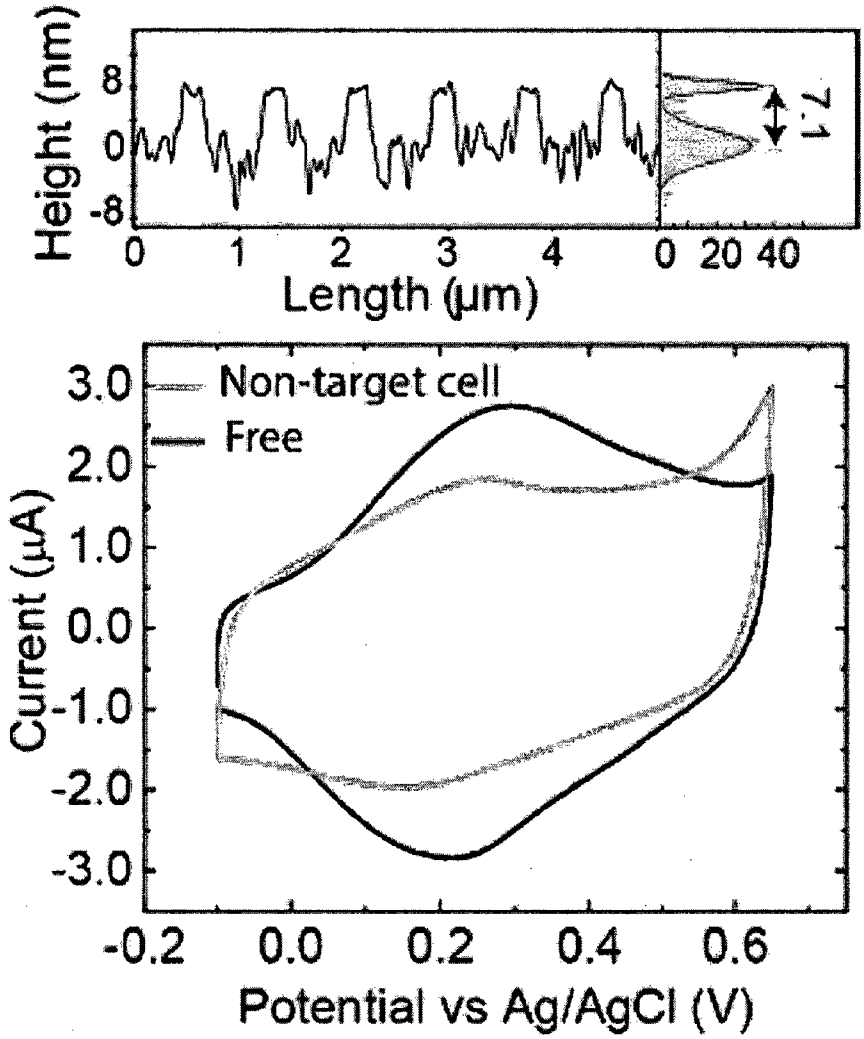
Height (nm)
8
0
-8
0 1 2 3 4
Length (μm)
0 20 40
1.1
Non-target cell
Free
Current (μA)
3.0
2.0
1.0
0.0
-1.0
-2.0
-3.0
-0.2 0.0 0.2 0.4 0.6
Potential vs Ag/AgCl (V)

[Figure 3b]

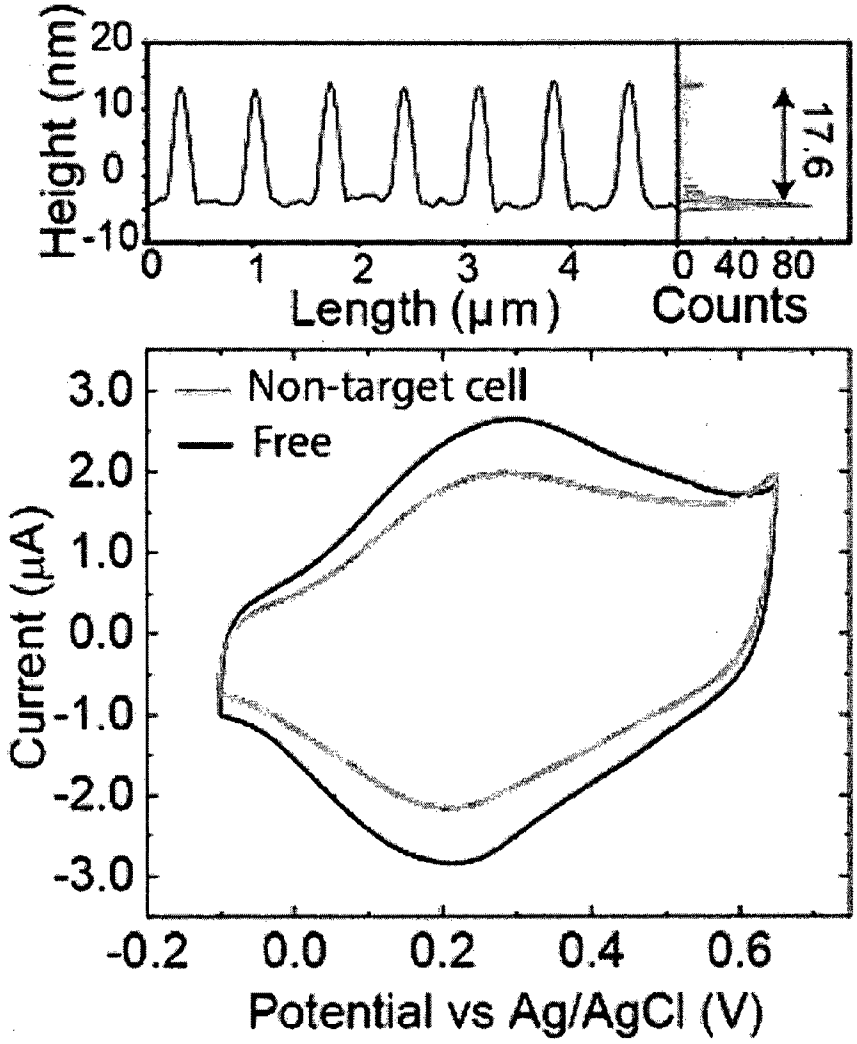
Height (nm)
20
10
0
-10
0
1
2
3
4
Length (μm)
17.6
0 40 80
Counts
Non-target cell
Free
Current (μA)
3.0
2.0
1.0
0.0
-1.0
-2.0
-3.0
-0.2
0.0
0.2
0.4
0.6
Potential vs Ag/AgCl (V)

[Figure 4]

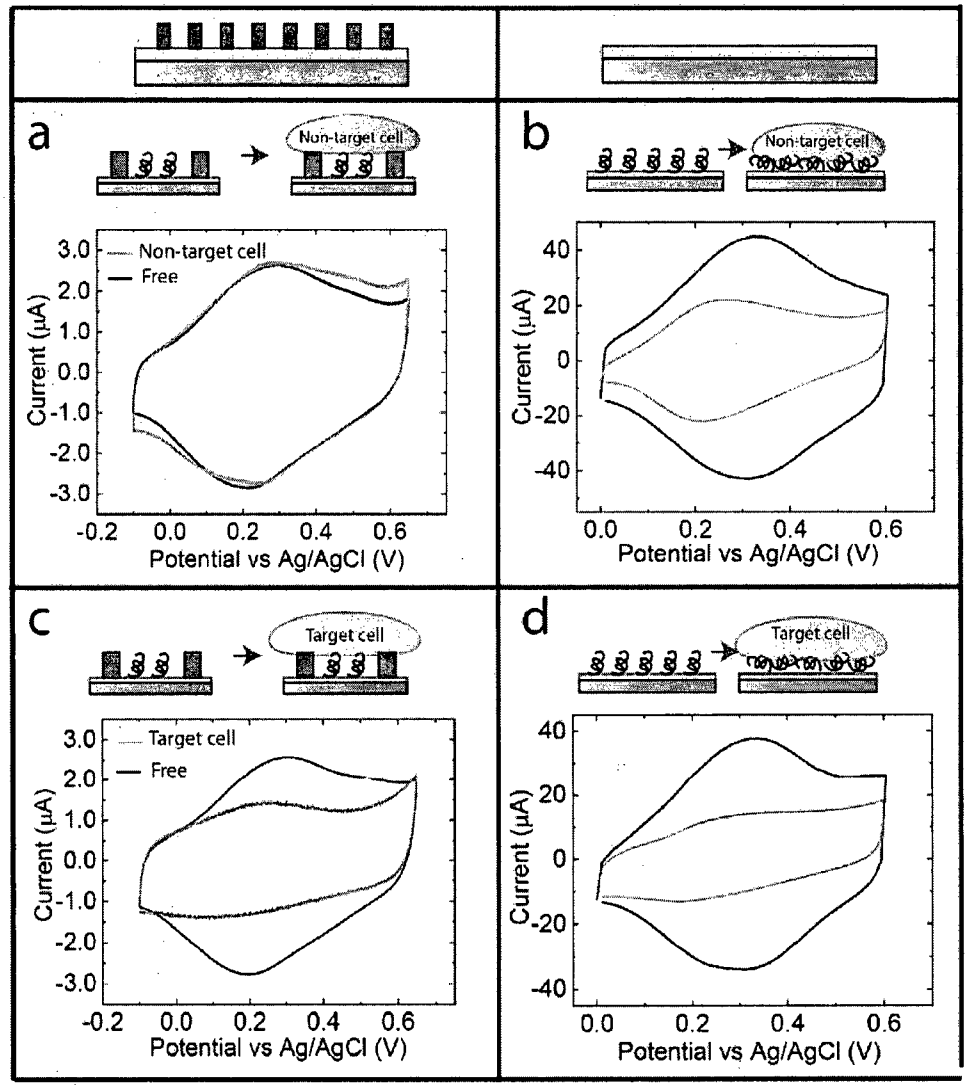
a
Non-target cell
Non-target cell
Free
Current (μA)
Potential vs Ag/AgCl (V)
b
Non-target cell
Current (μA)
Potential vs Ag/AgCl (V)
c
Target cell
Target cell
Free
Current (μA)
Potential vs Ag/AgCl (V)
d
Target cell
Current (μA)
Potential vs Ag/AgCl (V)

[Figure 5a]

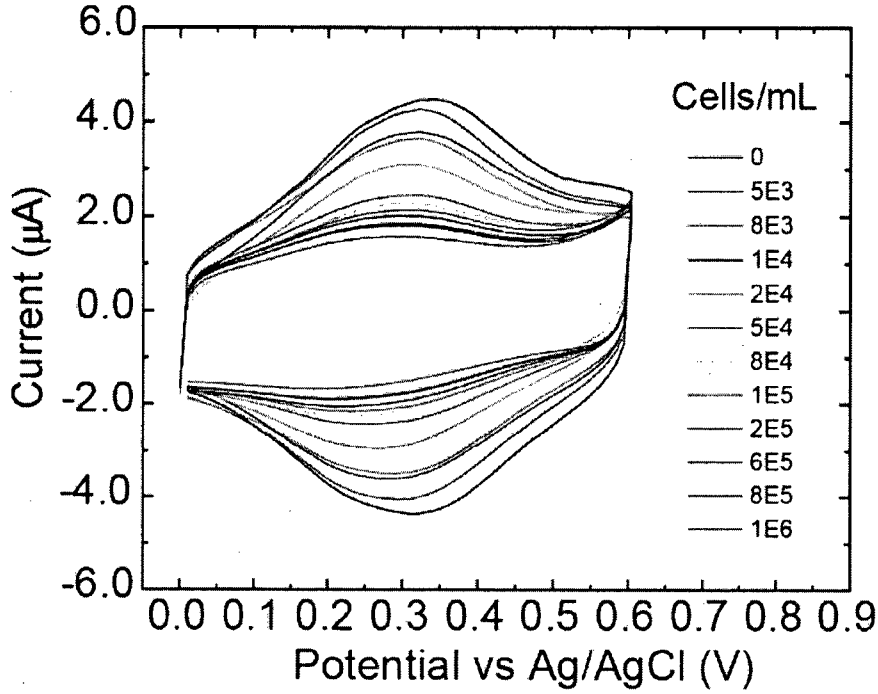
6.0
4.0
2.0
0.0
-2.0
-4.0
-6.0
Current (μA)
0.0 0.1 0.2 0.3 0.4 0.5 0.6 0.7 0.8 0.9
Potential vs Ag/AgCl (V)
Cells/mL
0
5E3
8E3
1E4
2E4
5E4
8E4
1E5
2E5
6E5
8E5
1E6

[Figure 5b]

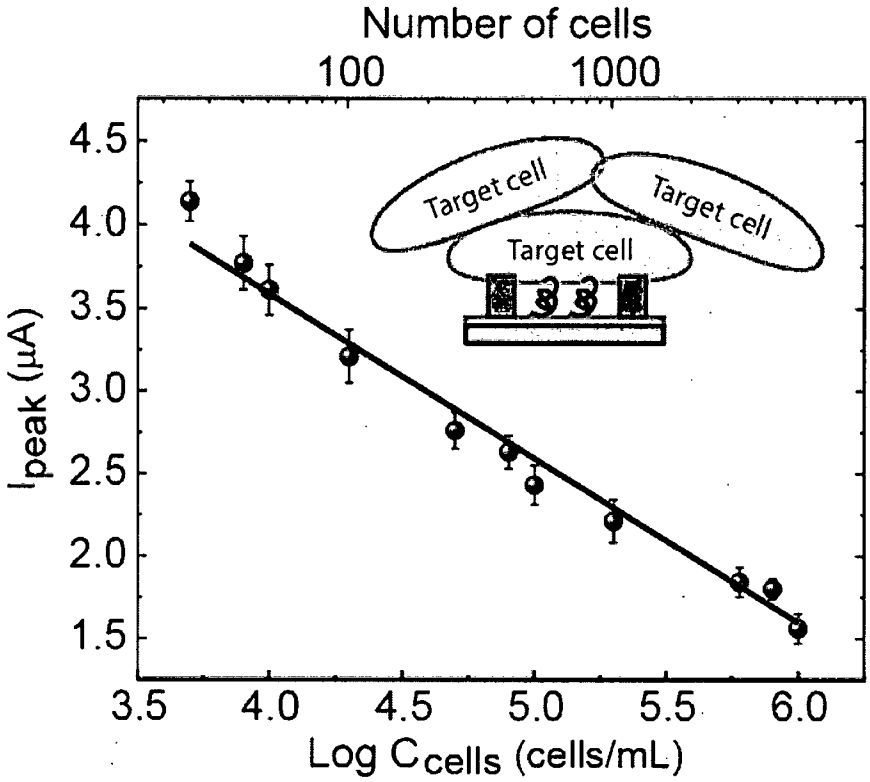
Number of cells
100
1000
4.5
4.0
3.5
3.0
2.5
2.0
1.5
Ipeak (μA)
3.5
4.0
4.5
5.0
5.5
6.0
Log Ccells (cells/mL)
Target cell
Target cell
Target cell

[Figure 6a]

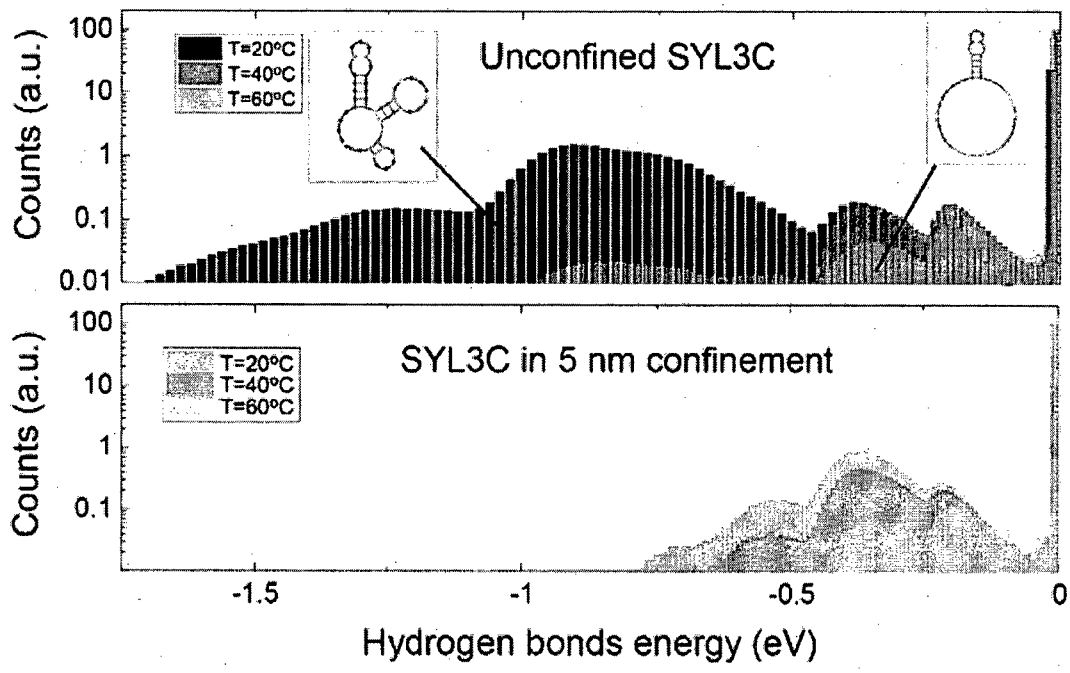
Unconfined SYL3C
T=20°C
T=40°C
T=60°C
Counts (a.u.)
100
10
1
0.1
0.01
SYL3C in 5 nm confinement
T=20°C
T=40°C
T=60°C
Counts (a.u.)
100
10
1
0.1
-1.5
-1
-0.5
0
Hydrogen bonds energy (eV)

[Figure 6b]

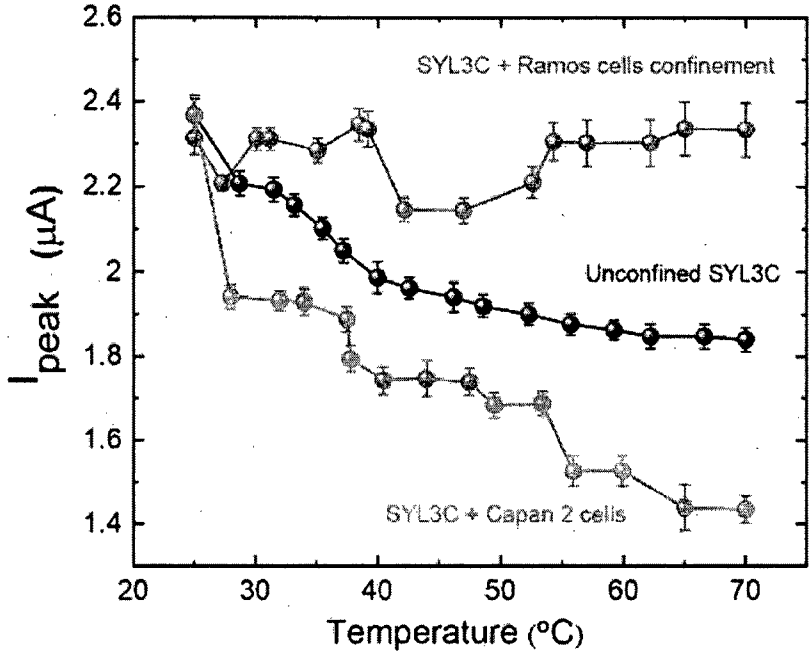
SYL3C + Ramos cells confinement
Unconfined SYL3C
SYL3C + Capan 2 cells
I_{peak} (μA)
Temperature (°C)
2.6
2.4
2.2
2
1.8
1.6
1.4
20
30
40
50
60
70

[Figure 7]

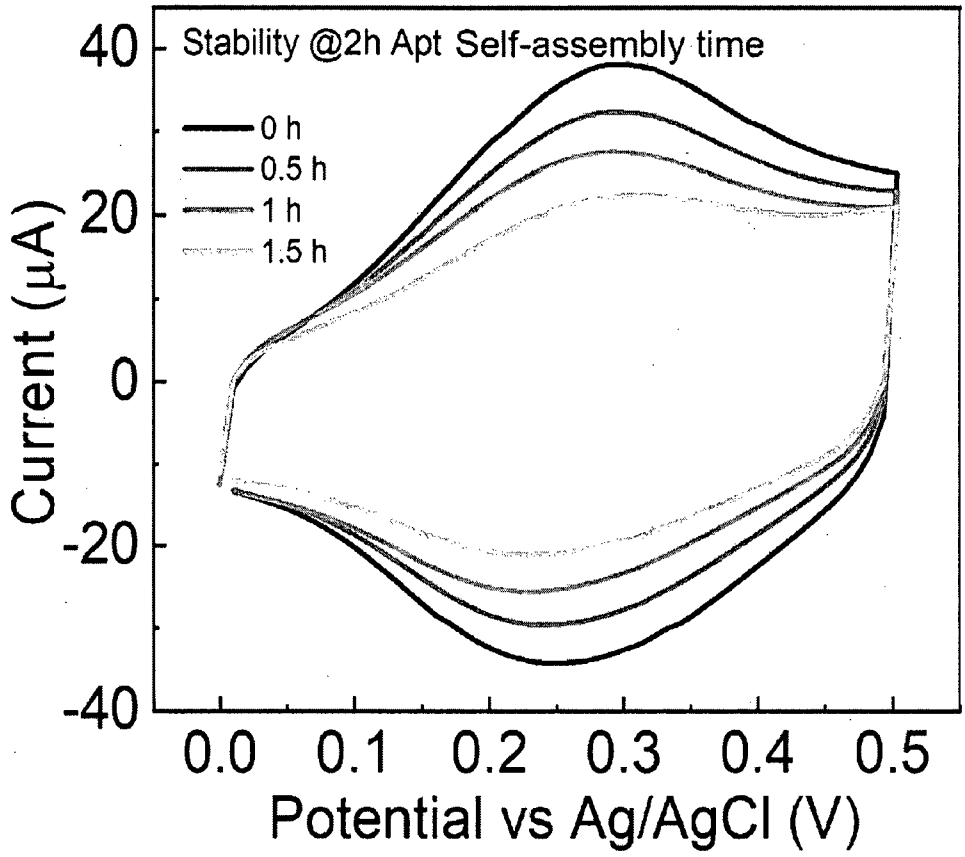
Stability @2h Apt Self-assembly time
0 h
0.5 h
1 h
1.5 h
Current (μA)
40
20
0
-20
-40
0.0
0.1
0.2
0.3
0.4
0.5
Potential vs Ag/AgCl (V)

[Figure 8]

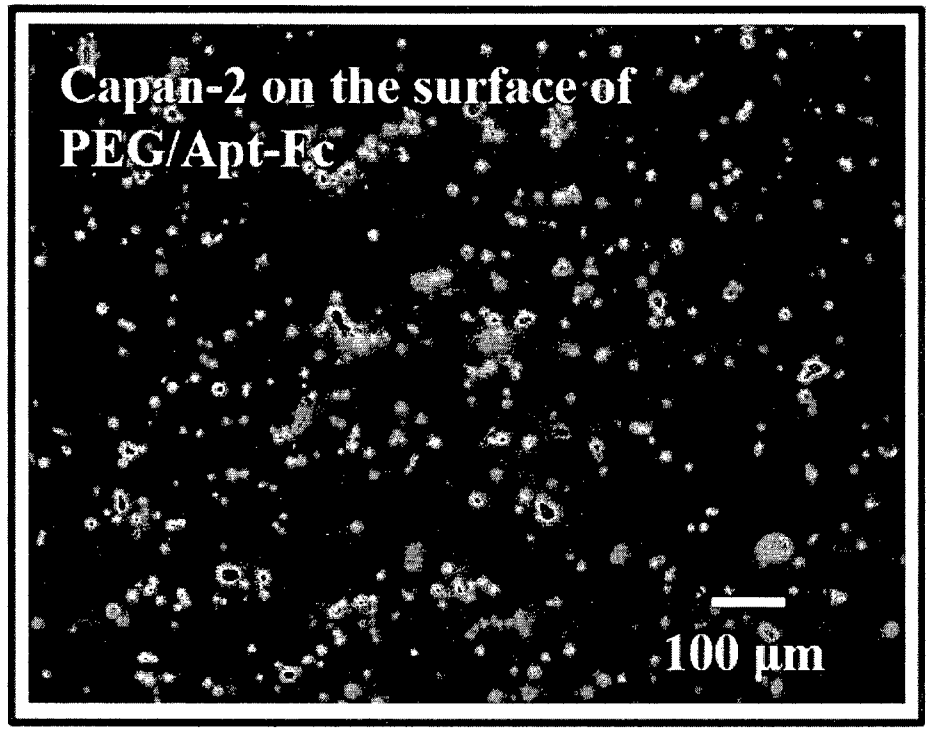

[Figure 9a]

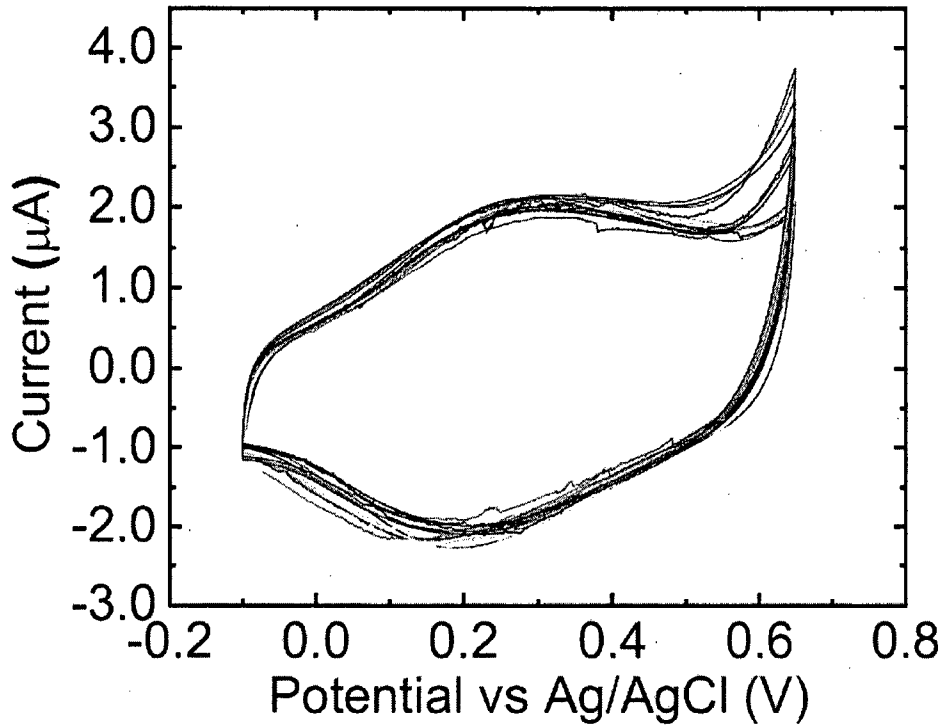
4.0
3.0
2.0
1.0
0.0
-1.0
-2.0
-3.0
Current (μA)
-0.2
0.0
0.2
0.4
0.6
0.8
Potential vs Ag/AgCl (V)

[Figure 9b]

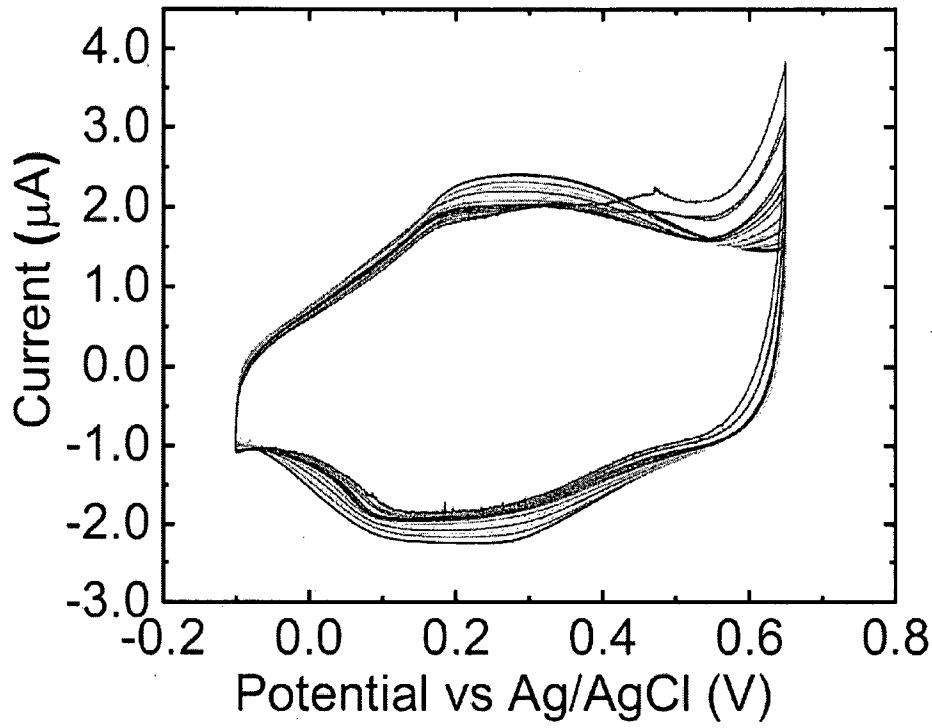
4.0
3.0
2.0
1.0
0.0
-1.0
-2.0
-3.0
Current (μA)
-0.2
0.0
0.2
0.4
0.6
0.8
Potential vs Ag/AgCl (V)

[Figure 9c]

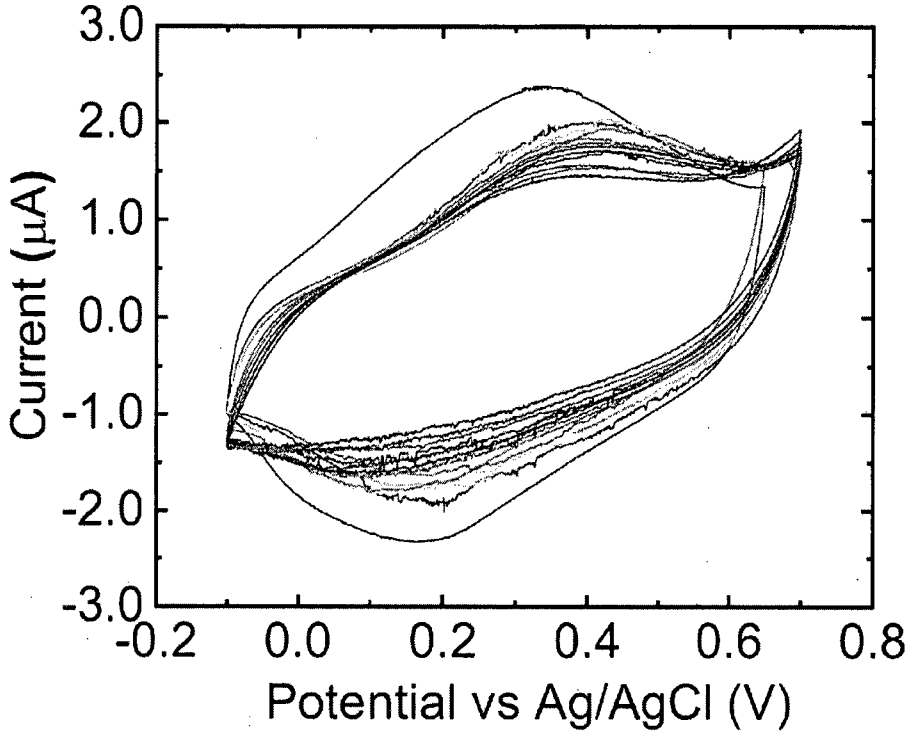
3.0
2.0
1.0
0.0
-1.0
-2.0
-3.0
Current (μA)
-0.2
0.0
0.2
0.4
0.6
0.8
Potential vs Ag/AgCl (V)

[Figure 10]

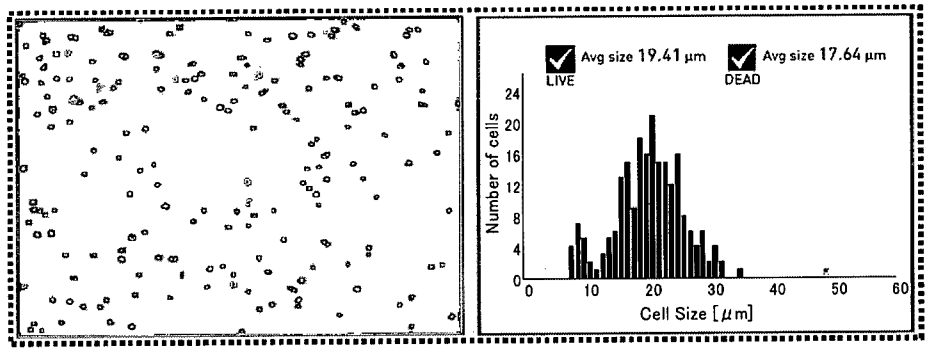

(a) Capan-2 cells

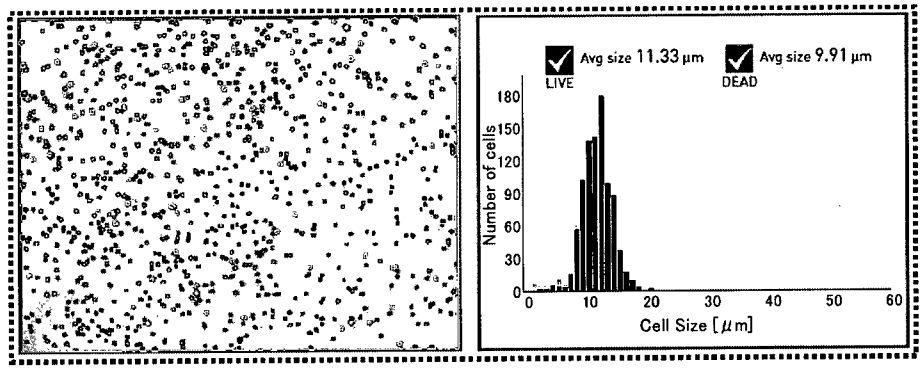

(b) Ramos cells

INTERNATIONAL SEARCH REPORT

International application No.
PCT/JP2022/020301

A. CLASSIFICATION OF SUBJECT MATTER

G01N 27/30(2006.01)i; ***G01N 27/416***(2006.01)i
FI: G01N27/416 336B; G01N27/30 F

According to International Patent Classification (IPC) or to both national classification and IPC

B. FIELDS SEARCHED

Minimum documentation searched (classification system followed by classification symbols)

G01N27/30; G01N27/416

Documentation searched other than minimum documentation to the extent that such documents are included in the fields searched

Published examined utility model applications of Japan 1922-1996
Published unexamined utility model applications of Japan 1971-2022
Registered utility model specifications of Japan 1996-2022
Published registered utility model applications of Japan 1994-2022

Electronic data base consulted during the international search (name of data base and, where practicable, search terms used)

JSTPlus/JMEDPlus/JST7580 (JDreamIII)

C. DOCUMENTS CONSIDERED TO BE RELEVANT

Category*	Citation of document, with indication, where appropriate, of the relevant passages	Relevant to claim No.
A	US 2020/0072825 A1 (DIGITAL SENSING LIMITED) 05 March 2020 (2020-03-05) Claims, Figures, [0056]	1-11
A	US 2020/0087810 A1 (MANUFACTURING SYSTEMS LIMITED) 19 March 2020 (2020-03-19) Claims, Figures	1-11
A	US 2019/0265236 A1 (KHALID, Waqas) 29 August 2019 (2019-08-29) Claims, Figures	1-11
A	US 2018/0100188 A1 (BOEHRINGER INGELHEIM VETMEDICA GMBH) 12 April 2018 (2018-04-12) Claims, Figures	1-11
A	JP 2012-37397 A (CANON INC.) 23 February 2012 (2012-02-23) Claims, Figures	1-11

☐ Further documents are listed in the continuation of Box C. ☑ See patent family annex.

* Special categories of cited documents:
"A" document defining the general state of the art which is not considered to be of particular relevance
"E" earlier application or patent but published on or after the international filing date
"L" document which may throw doubts on priority claim(s) or which is cited to establish the publication date of another citation or other special reason (as specified)
"O" document referring to an oral disclosure, use, exhibition or other means
"P" document published prior to the international filing date but later than the priority date claimed
"T" later document published after the international filing date or priority date and not in conflict with the application but cited to understand the principle or theory underlying the invention
"X" document of particular relevance; the claimed invention cannot be considered novel or cannot be considered to involve an inventive step when the document is taken alone
"Y" document of particular relevance; the claimed invention cannot be considered to involve an inventive step when the document is combined with one or more other such documents, such combination being obvious to a person skilled in the art
"&" document member of the same patent family

Date of the actual completion of the international search	Date of mailing of the international search report
06 July 2022	**19 July 2022**
Name and mailing address of the ISA/JP **Japan Patent Office** **3-4-3, Kasumigaseki, Chiyoda-ku, Tokyo** **100-8915, Japan**	Authorized officer **OTAKI, Mari 2J 9812** Telephone No. **+81-3-3581-1101 Ext. 3252**

INTERNATIONAL SEARCH REPORT
Information on patent family members

International application No.
PCT/JP2022/020301

Patent document cited in search report	Publication date (day/month/year)	Patent family member(s)	Publication date (day/month/year)
US 2020/0072825 A1	05 March 2020	JP 2020-502502 A	
		WO 2018/106129 A1	
		CN 110140043 A	
US 2020/0087810 A1	19 March 2020	JP 2020-517817 A	
		WO 2018/106128 A1	
		CN 110073038 A	
US 2019/0265236 A1	29 August 2019	JP 2019-514022 A	
		WO 2017/173042 A2	
		CN 109641742 A	
		KR 10-2019-0034139 A	
US 2018/0100188 A1	12 April 2018	JP 2019-536441 A	
		WO 2018/065104 A1	
		KR 10-2019-0066037 A	
		CN 110114145 A	
JP 2012-37397 A	23 February 2012	(Family: none)	